

Nonlinear response of the vacuum Rabi resonance

Lev S. Bishop,¹ J. M. Chow,¹ Jens Koch,¹ A. A. Houck,¹ M. H. Devoret,¹ E. Thuneberg,² S. M. Girvin,¹ and R. J. Schoelkopf^{1,*}

¹*Departments of Physics and Applied Physics, Yale University, PO Box 208120, New Haven, CT 06520, USA*

²*Department of Physical Sciences, University of Oulu, PO Box 3000, FI-90014, Finland*

(Dated: 26th October 2018)

On the level of single atoms and photons, the coupling between atoms and the electromagnetic field is typically very weak. By employing a cavity to confine the field, the strength of this interaction can be increased many orders of magnitude to a point where it dominates over any dissipative process. This strong-coupling regime of cavity quantum electrodynamics (QED)^{1,2}, has been reached for real atoms in optical cavities³, and for artificial atoms in circuit QED⁴ and quantum-dot systems^{5,6}. A signature of strong coupling is the splitting of the cavity transmission peak into a pair of resolvable peaks when a single resonant atom is placed inside the cavity – an effect known as vacuum Rabi splitting. The circuit QED architecture is ideally suited for going beyond this linear response effect. Here, we show that increasing the drive power results in two unique nonlinear features in the transmitted heterodyne signal: the supersplitting of each vacuum Rabi peak into a doublet, and the appearance of additional peaks with the characteristic \sqrt{n} spacing of the Jaynes–Cummings ladder. These constitute direct evidence for the coupling between the quantized microwave field and the anharmonic spectrum of a superconducting qubit acting as an artificial atom.

Circuit QED realizes the coupling between a superconducting qubit and the microwave field inside an on-chip transmission line resonator^{4,7}. The drastic reduction in mode volume for such a quasi-1d system^{8,9}, the recent improvement in coherence times¹⁰, and the absence of atomic motion render circuit QED an ideal system for studying the strong-coupling limit. In the customary linear-response measurement of the transmitted microwave radiation, the vacuum Rabi splitting manifests itself as an avoided crossing between qubit and resonator.

It may be argued that the observation of the splitting is not yet a clear sign for quantum behaviour^{11,12}, since avoided crossings are also ubiquitous in classical physics. However, quantum mechanics gives rise to a distinct nonlinearity of these splittings when initializing the resonator in a higher photon Fock state: when the resonator mode is occupied by n photons, the splitting is enhanced by a factor $\sqrt{n+1}$ as compared to the vacuum Rabi situation. This nonlinearity has been observed with single atoms in both microwave¹³ and optical cavities^{14,15}. In circuit QED, this characteristic trait has been observed very recently both spectroscopically¹⁶, as well as in time-domain measurements^{17,18}.

Here, we present a theoretical analysis and experimental investigation of the vacuum Rabi resonance in a circuit QED system, where we study the \sqrt{n} nonlinearity up to $n = 5$ by exploring the power dependence of the

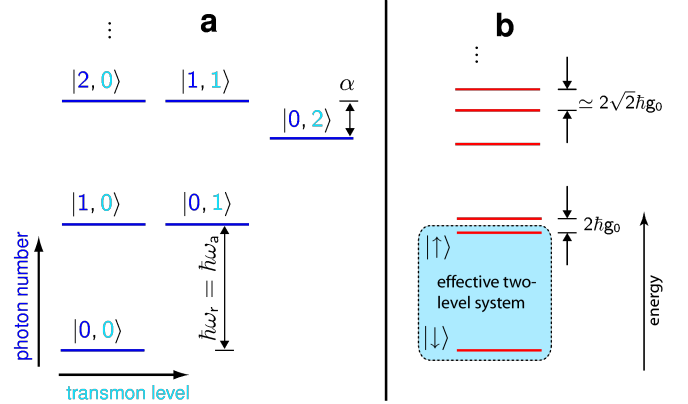


Figure 1: **Extended Jaynes–Cummings level diagram of the resonator–transmon system.** **a**, Bare levels in the absence of coupling. The states are denoted $|n, j\rangle$ for photon number n and occupation of transmon level j . **b**, Spectrum of the system including the effects of transmon–resonator coupling. The effective two-level system relevant to describing the lower vacuum Rabi peak comprises the ground state and the antisymmetric combination of qubit and photon excitations.

heterodyne transmission (see Methods). This type of detection is particularly simple, since it is a continuous measurement involving only a single driving frequency. We find that, surprisingly, each vacuum Rabi peak develops into a new doublet (supersplitting), which can be simply explained by the saturation of a two-level system comprising both photon and qubit degrees of freedom. For even stronger driving, a series of additional peaks due to multiphoton transitions¹⁹ up the Jaynes–Cummings ladder appear, but the complete shape of the spectrum closely matches the predictions from a master equation treatment including only relaxation, dephasing, and the known multilevel spectrum of the superconducting qubit. The quantitative agreement confirms the validity of the extended Jaynes–Cummings Hamiltonian for our system, rendering circuit QED an excellent tool for probing the fundamental interaction of matter and light.

We consider a system consisting of a superconducting transmon qubit^{10,20} whose multiple quantum levels are coupled to a single mode of a transmission-line resonator. Our arguments, however, will be general and should apply to any other realization of cavity QED with sufficiently large coupling and atom coherence times. Taking into account the relatively small anharmonicity of the

transmon qubit, the system is modelled in terms of an extended Jaynes–Cummings hamiltonian including a coherent drive at frequency $\omega_d/2\pi$,

$$H = \hbar\omega_r a^\dagger a + \sum_j \hbar\omega_j |j\rangle \langle j| \quad (1)$$

$$+ \sum_j \hbar g_j (a |j+1\rangle \langle j| + \text{h.c.}) + \hbar\xi (a^\dagger e^{-i\omega_a t} + \text{h.c.}).$$

Here, the operator a (a^\dagger) annihilates (creates) a photon in the resonator mode with frequency $\omega_r/2\pi$. The energies corresponding to the transmon eigenstates are $\hbar\omega_j$ ($j = 0, 1, \dots$), and they are determined by the Cooper pair box hamiltonian²¹ for given Josephson energy E_J and charging energy E_C . In the transmon regime considered here, $E_J/E_C \gg 1$, the levels form a weakly anharmonic ladder with anharmonicity $\alpha = \omega_{12} - \omega_{01} \sim -E_C$ ($\omega_{ij} = \omega_j - \omega_i$ is the transition frequency between levels i and j). The transmon–resonator coupling strengths are $g_j \sim g_0\sqrt{j+1}$, where $g_0/2\pi$ is the vacuum Rabi frequency. The resulting energy level diagram for vanishing drive, $\xi = 0$, is schematically shown in Fig. 1.

The interaction of the cavity–transmon system with its environment enables control and measurement by means of microwave drive and detection^{4,7}, but also leads to decoherence. The appropriate framework to capture all these effects is a description in terms of the reduced density matrix ρ for the cavity and transmon. The Markovian master equation which governs the evolution of ρ is given by

$$\dot{\rho} = -\frac{i}{\hbar} [H, \rho] + \kappa \mathcal{D}[a]\rho + \gamma_1 \mathcal{D}\left[\sum_j \alpha_j |j\rangle \langle j+1|\right]\rho$$

$$+ \frac{\gamma_\varphi}{2} \mathcal{D}\left[\sum_j \beta_j |j\rangle \langle j|\right]\rho, \quad (2)$$

where $\mathcal{D}[A]$ is the usual Lindblad damping superoperator defined by $\mathcal{D}[A]\rho = ([A\rho, A^\dagger] + [A, \rho A^\dagger])/2$. The three damping terms on the right-hand side model the loss of cavity photons at rate κ , the intrinsic relaxation of transmon excitations at rate γ_1 , and the pure dephasing of transmon state superpositions at rate γ_φ and relative strengths α_j, β_j (see Methods).

The quantity of interest for detection of the vacuum Rabi splitting is the transmission amplitude $A(\omega_d)$ of a microwave signal at frequency $\omega_d/2\pi$. Here, we employ a heterodyne measurement of the field quadratures $I = \langle b_{\text{out}} + b_{\text{out}}^\dagger \rangle$ and $Q = \langle ib_{\text{out}}^\dagger - ib_{\text{out}} \rangle$, where b_{out} refers to the output field at the drive frequency. Input-output theory²² enables us to express the steady-state transmission amplitude as

$$A = \sqrt{I^2 + Q^2} = 2\sqrt{\kappa} |\langle a \rangle| = 2\sqrt{\kappa} |\text{tr}(a \rho_s)|. \quad (3)$$

Our calculations thus only require the steady-state solution ρ_s of the master equation (2). We explore the transmission intensity A^2 as a function of the drive strength

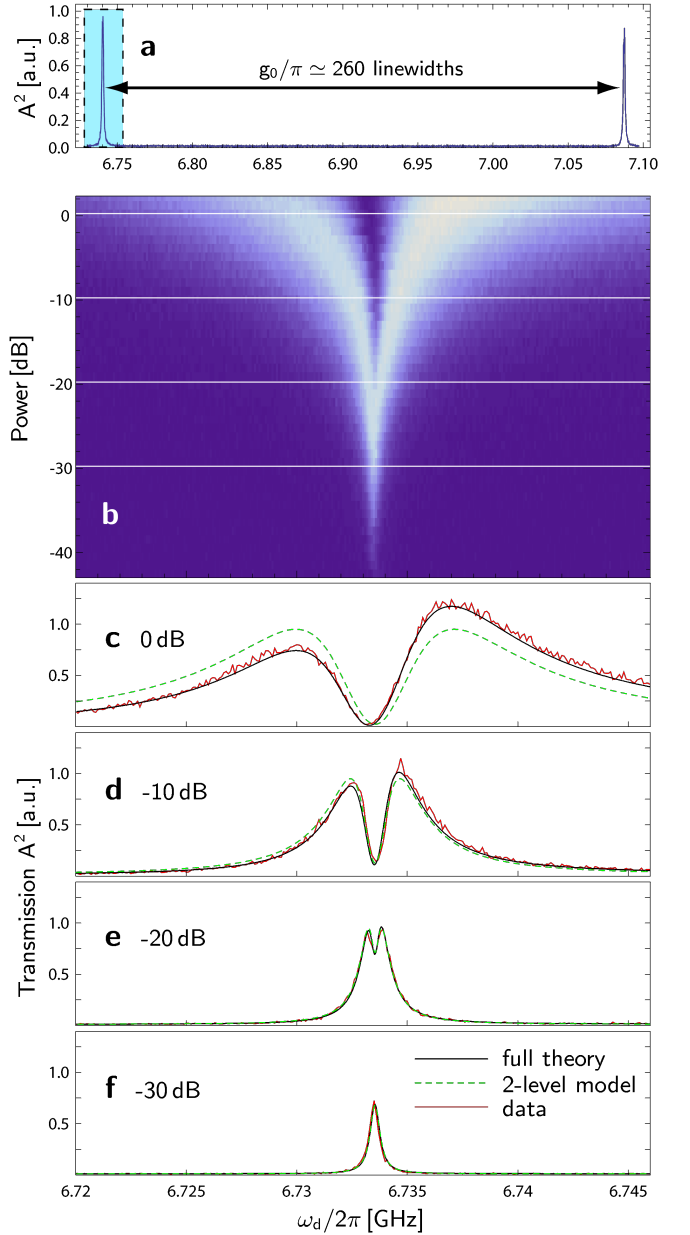


Figure 2: Supersplitting of the vacuum Rabi resonance when probing heterodyne transmission beyond linear response. The experimental data are obtained with a circuit QED system in the strong-coupling regime, where the vacuum Rabi splitting is observed to exceed 260 linewidths, see **a**. All plots show the squared heterodyne amplitude A^2 in arbitrary units. **b**, Measured transmission (colour scale) for the left vacuum Rabi peak, as a function of drive frequency and power. The plot reveals the supersplitting of a single Lorentzian into a doublet of peaks. **c–f**, Cuts for constant power at the values indicated in **b**. In linear response, **f**, the vacuum Rabi peak is Lorentzian; as the power increases a central dip develops, **e**, leading to supersplitting of the peak, **d**, and eventually becoming asymmetric at the largest powers, **c**. The experimental data (red line) is in excellent agreement with theory (black line). The results from the 2-level approximation are shown for comparison (green dashed line).

ξ , and compare our results to experimental data obtained for a transmon qubit in resonance with a $\omega_r/2\pi = 6.92$ GHz coplanar waveguide (CPW) resonator with coupling strength $g_0/\pi = 347$ MHz (see Methods for experimental details). In the linear-response regime, the vacuum Rabi peaks have the characteristic Lorentzian line shape. Their separation and width are given by $2g_0$ and $(\gamma_1 + 2\gamma_\varphi + \kappa)/2$, respectively. For our specific sample, the splitting is observed to exceed 260 linewidths, shown in Fig. 2a. Strikingly, when increasing the drive power beyond the linear-response regime, the shape of the transmission curve changes drastically as shown in Figs. 2b–f. Each vacuum Rabi peak develops a central dip and eventually supersplits into a doublet of peaks. We find excellent agreement between our prediction based on Eqs. (2) and (3) and the measured transmission.

The physics of this supersplitting can be elucidated within a reduced two-level model. This model takes into account only the Jaynes–Cummings ground state and either the symmetric or antisymmetric superposition of transmon and photon excitation. These two states, $|\downarrow\rangle = |0, 0\rangle$ and $|\uparrow\rangle = (|1, 0\rangle \pm |0, 1\rangle)/\sqrt{2}$, form an effective two-level system composed of both transmon and cavity degrees of freedom. Within the effective two-level subspace, the photon operators are mapped²³ to Pauli operators $a \rightarrow \Sigma_-/\sqrt{2}$, $a^\dagger \rightarrow \Sigma_+/\sqrt{2}$, so that the microwave tone acts as a drive on the effective two-level system, i.e.

$$H_{\text{eff}} = \frac{\hbar\Delta}{2}\Sigma_z + \frac{\hbar\Omega}{2}\Sigma_x, \quad (4)$$

a scenario that Carmichael et al.^{12,23} have referred to as “dressing of dressed states.” The hamiltonian H_{eff} refers to the frame rotating at the drive frequency, $\Delta = \omega_{01} \pm g_0 - \omega_d$ is the detuning between drive and one vacuum Rabi peak, and $\Omega = \sqrt{2}\xi$ is the effective drive strength. With the notable exception of the recent work by I. Schuster et al.¹⁴, previous investigations were primarily concerned with effects on photon correlations and fluorescence, as observed in photon-counting measurements^{12,15}. According to the operator mapping, photon counting can be related to the measurement of $\langle\Sigma_z\rangle$, whereas detection of the heterodyne transmission amplitude A corresponds to $|\langle\Sigma_- \rangle|$. As a result, heterodyne detection fundamentally differs from photon counting and the vacuum Rabi supersplitting is a characteristic of heterodyne detection only.

After restricting the master equation (2) to the two-level subspace, the system evolution can be expressed in terms of simple Bloch equations for the three components of the reduced density matrix $\rho = (\mathbb{1} + x\Sigma_x + y\Sigma_y + z\Sigma_z)/2$,

$$\begin{aligned} \dot{x} &= -x/T_2' - \Delta y, & \dot{y} &= \Delta x - y/T_2' - \Omega z, \\ \dot{z} &= \Omega y - (z + 1)/T_1'. \end{aligned} \quad (5)$$

(An intuitive approach avoiding the Bloch equations is discussed in the Supplementary Information, Discussion.) Here, T_1' and T_2' are the effective relaxation and

dephasing times, which are related to γ_1 , γ_φ , and κ via $T_1'^{-1} = (\gamma_1 + \kappa)/2$, and $T_2'^{-1} = (\gamma_1 + 2\gamma_\varphi + \kappa)/4$. From the steady-state solution of the Bloch equations we find the transmission amplitude

$$A = \frac{T_2'\Omega\sqrt{\kappa(\Delta^2 T_2'^2 + 1)}/2}{\Delta^2 T_2'^2 + T_1' T_2' \Omega^2 + 1}. \quad (6)$$

This expression correctly describes the crossover from linear response at small driving strength, $\Omega \ll (T_1' T_2')^{-1/2}$, producing a Lorentzian of width $2T_2'^{-1}$, to the doublet structure observed for strong driving. Specifically, as the drive power is increased, the response saturates and the peak broadens, until at $\Omega = (T_1' T_2')^{-1/2}$ the peak undergoes supersplitting with peak–peak separation $2T_2'^{-1}\sqrt{T_1' T_2' \Omega^2 - 1}$. The fact that we use heterodyne detection is indeed crucial for the supersplitting. It is easy to verify within the two-level approximation that photon-counting always results in a Lorentzian. For photon counting, probing beyond the linear-response regime merely results in additional power-broadening; specifically, the width of the Lorentzian is given by $2T_2'^{-1}\sqrt{T_1' T_2' \Omega^2 + 1}$.

In Figs. 2c–e, the analytical expression (6) is plotted for comparison with the full numerical results and the experimental data. We find good agreement for low to moderate drive power, confirming that the supersplitting can be attributed to driving the vacuum Rabi transition into saturation while measuring the transmission with the heterodyne technique. For higher drive power a left-right asymmetry appears in the true transmission spectrum, which is not reproduced by Eq. (6), and which is partly due to the influence of levels beyond the two-level approximation.

Higher levels of the extended Jaynes–Cummings hamiltonian become increasingly important when the drive power is raised further. Figure 3 shows the emergence of additional peaks in the transmission spectrum. Each of the peaks can be uniquely identified with a multiphoton transition from the ground state to an excited Jaynes–Cummings state. For simplicity, we consider the situation where the anharmonicity α and the coupling strength g_0 are sufficiently different that mixing between higher transmon levels and the regular Jaynes–Cummings states $|n, \pm\rangle = (|n+1, 0\rangle \pm |n, 1\rangle)/\sqrt{2}$ is minimal for the low-excitation subspaces. Accordingly, the experiments are carried out using a different transmon qubit in the same sample, with a smaller coupling of $g_0/\pi = 94.4$ MHz (see Methods). In this case, the n -photon transitions to the n -excitation subspace occur at frequencies $E_{n\pm}/nh = (\omega_r \pm n^{-1/2}g_0)/2\pi$, and thus reveal the nonlinearity of the Jaynes–Cummings ladder. The detailed comparison between experimental data and numerical simulation in Fig. 3c–e shows superb agreement down to the narrowest features observed.

The possibility of multiphoton transitions at sufficiently large drive powers also affects the shape of the vacuum Rabi splitting when tuning the qubit frequency

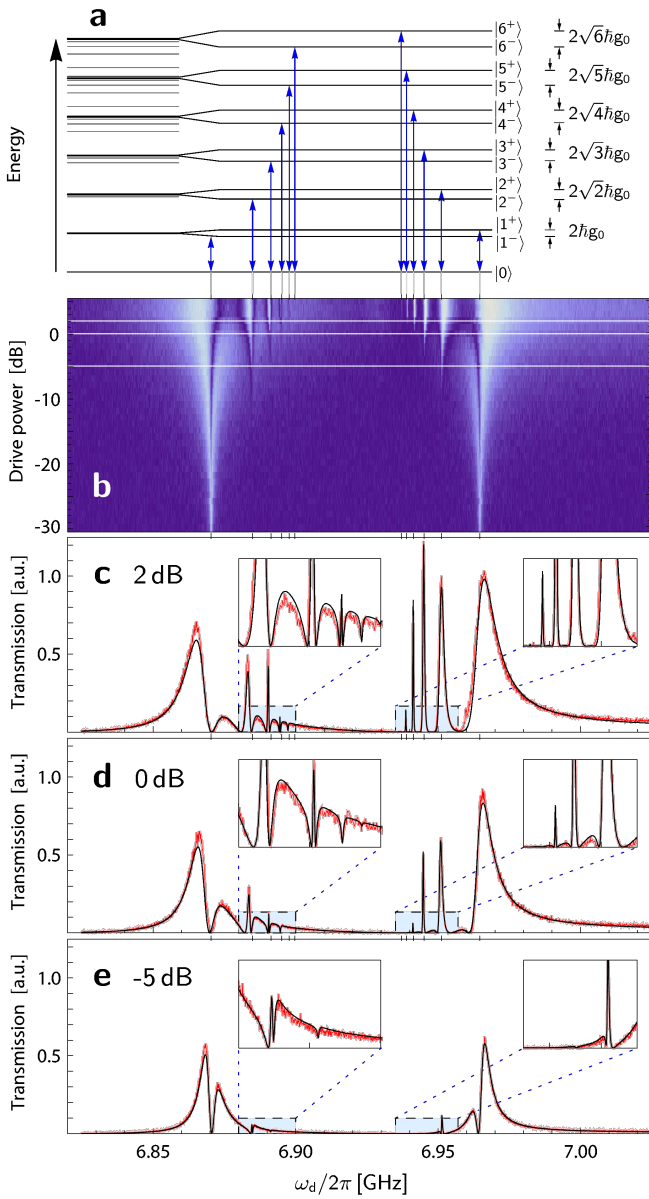


Figure 3: Emergence of \sqrt{n} peaks under strong driving of the vacuum Rabi transition. **a**, The extended Jaynes-Cummings energy spectrum. All levels are shown to scale in the left part of the diagram: black lines represent levels $|n, \pm\rangle \simeq (|n+1, 0\rangle \pm |n, 1\rangle)/\sqrt{2}$ with only small contributions from higher ($j > 1$) transmon states; grey lines represent levels with large contributions from higher transmon states. In the right part of the diagram, the \sqrt{n} scaling of the splitting between the $|n, \pm\rangle$ states is exaggerated for clarity, and the transitions observed in plots **b–e** are indicated at the x -coordinate $E_{n\pm}/n\hbar$ of their n -photon transition frequency from the ground state. **b**, Measured transmission (A^2 , heterodyne amplitude squared) in colour scale as a function of drive frequency and power. The multiphoton transitions shown in **a** are observed at their calculated positions. **c–e**, Examples of cuts for constant power, at the values indicated in **b** (results from the master equation (2) in black; experimental results in red), demonstrating excellent agreement between theory and experiment, which is reinforced in the enlarged insets. Good agreement is found over the full range in drive power from -45 dB to $+3$ dB, for a single set of parameters (also see Supplementary Movie 1).

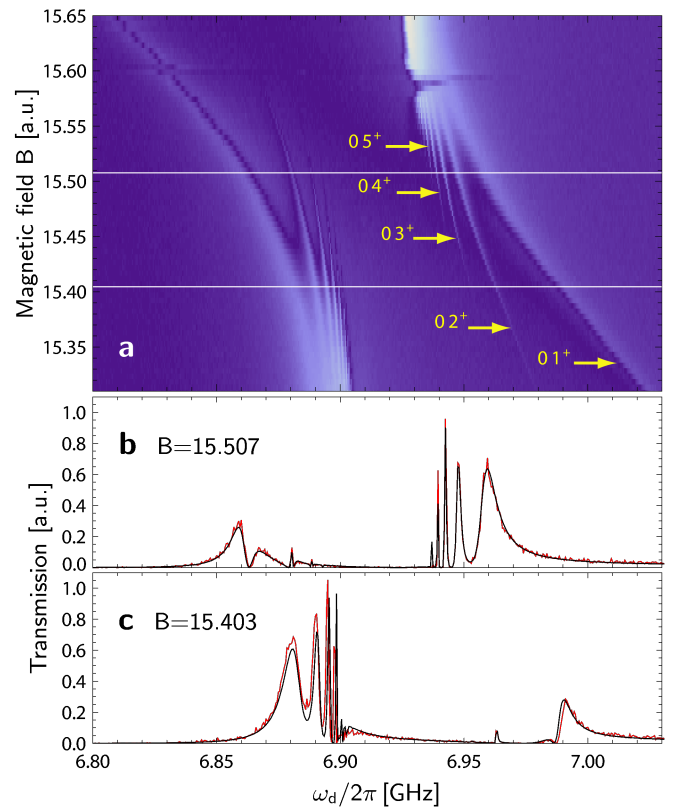


Figure 4: Qubit-cavity avoided crossing at high drive power. Transmission measurement when tuning the qubit frequency through resonance for a drive power of $+1$ dB. **a**, Measured transmission as a function of drive frequency and magnetic field. As the field is increased, the qubit frequency is tuned through resonance with the cavity, and anticrossing behaviour is observed. The multiphoton transitions shown in Fig. 3a are visible. The anomaly at $B \simeq 15.59$ is most likely due to the crossing of a higher level of the second qubit present in the same cavity. **b–c**, Example cuts at constant magnetic field, at the values indicated in **a** (master equation results, calculated using the same parameters as for Fig. 3, are shown in black; measured results in red). (Also see Supplementary Movie 2).

ω_{01} through resonance with the cavity, shown in Fig. 4. Instead of the simple avoided crossing commonly observed at low drive powers⁴, the presence of multiphoton transitions leads to a fan-like structure where individual branches can again be identified one-to-one with the possible transitions in the Jaynes-Cummings ladder. In the experimental data of Fig. 4a, processes up to the 5-photon transition are clearly visible. Detailed agreement with the theory verifies that the more general situation of non-zero detuning between qubit and resonator is correctly described by our model.

In summary, we have shown the supersplitting and the emergence of multiphoton transitions in the nonlinear response of the vacuum Rabi resonance, presenting both theoretical predictions and their experimental verification. This enables the observation of the character-

istic \sqrt{n} nonlinearities in the Jaynes–Cummings ladder in a heterodyne transmission measurement, and is direct evidence for the strong coupling between the superconducting qubit and the quantized microwave field. The high precision of agreement between predictions and experiment demonstrates the robustness of the Jaynes–Cummings physics in a circuit QED system. This opens up pathways for further investigations in quantum optics and quantum information, such as generating number-squeezed states or employing multi-level quantum logic.

METHODS

THEORY

The modelling of the transmon follows ref. 20. While some expressions given in the main text are asymptotic results valid for $E_J/E_C \gg 1$, our calculations are based on a full diagonalization of the Cooper pair box Hamiltonian.

The description of the transmon–cavity system in terms of a master equation requires a model for the relaxation and dephasing of higher transmon levels. As detailed studies of the microscopic origin of the dominant relaxation and dephasing channels are still outstanding, we have chosen plausible superoperators for our master equation (2). Assuming that relaxation of higher transmon levels may arise due to a coupling of external degrees of freedom to the charge on the superconducting island, we take the relative strengths of relaxation to be related to the coupling parameters as $\alpha_j = g_j/g_0$. Dephasing of higher levels is likely to be due to charge noise. Denoting the charge dispersion²⁰ of level j by $\epsilon_j = \omega_j(n_g = 0) - \omega_j(n_g = 1/2)$, we therefore take the relative dephasing strengths to be $\beta_j = 2\epsilon_j/(\epsilon_1 - \epsilon_0)$. (The normalisation of α_j and β_j is chosen to allow the usual interpretation of γ_1 and γ_φ as relaxation and dephasing rates for the first two levels of the transmon spectrum.) In fact, the pure dephasing rate is sufficiently small for our qubits that we set $\gamma_\varphi = 0$. A comparison of additional simulations with auxiliary experimental results at increased temperatures allows us to place an approximate upper bound of 0.003 on the number of thermal photons in the cavity.

For the steady-state solution of Eq. (2), the Hilbert space is truncated to a subspace with maximum number of excitations N , using the projector $P_N = \sum_{0 \leq n+j \leq N} |n, j\rangle \langle n, j|$. In our simulations, we keep up

to $N = 7$ excitations. To reach agreement with the experimentally measured signal for the strongest drive powers, it is necessary to account for a small amount (~ -55 dB) of leakage of the drive past the cavity. In addition, there is a small bias introduced by measuring the transmission as the square of the I and Q quadratures, each of which is subject to noise. Accordingly, the quantity that corresponds to the experimental signal is $A^2 = |2\sqrt{\kappa} \text{tr}(\rho_s a) + b\xi|^2 + 2\sigma_n^2$, where b describes the leakage of the drive bypassing the cavity, and σ_n is the measurement noise in each of the I and Q channels.

Fits are obtained by minimizing the mean squared deviation between experiment and calculation over the full power range, with fit parameters being b and the two scaling factors describing the signal attenuation and amplification for input and output signals. To obtain optimal agreement, we also make small adjustments to the system parameters γ_1 , κ , g_0 , ω_r , ω_{01} , and E_C . These parameters are confined by separate experiments to narrow ranges, and all values used in fits are consistent within the experimental uncertainties. Once obtained, the same set of parameters was used in generating Figs. 3, 4, and the Supplementary Movies.

EXPERIMENT

Measurements are performed in a dilution refrigerator at 15 mK. The sample consists of two superconducting transmon qubits^{10,20}, coupled to an on-chip coplanar waveguide (CPW) cavity. Fabrication of the sample followed the description given in ref. 10. The CPW resonator has a half-wavelength resonant frequency of $\omega_r/2\pi = 6.92$ GHz and a photon decay rate of $\kappa/2\pi = 300$ kHz. Transmission measurements are performed using a heterodyne detection scheme. The transmitted RF voltage signal through the cavity is mixed down to a 1 MHz carrier signal, and then digitally mixed down to dc to obtain the transmitted voltage amplitude as a function of frequency. The vacuum Rabi coupling strengths for the two qubits are obtained as $g_0/\pi = 347$ MHz (qubit 1) and $g_0/\pi = 94.4$ MHz (qubit 2). Time domain measurements of the qubits show that they are Purcell-limited and completely homogeneously broadened at their flux sweet spots²⁴. The coherence times are $T_1 = 1.7 \mu\text{s}$ and $T_2 = 0.7 \mu\text{s}$ (qubit 1, away from the flux sweet spot) and $T_1 = 1.4 \mu\text{s}$ and $T_2 = 2.8 \mu\text{s}$ (qubit 2, at flux sweet spot). The charging energies of the two qubits are measured to be $E_C/h = 400$ MHz and $E_C/h = 340$ MHz. (See Supplementary Information, Methods, for further details.)

* email: robert.schoelkopf@yale.edu

¹ Raimond, J. M., Brune, M., and Haroche, S. Manipulating quantum entanglement with atoms and photons in a cavity. *Rev. Mod. Phys.* **73**, 565 (2001).

² Miller, R., Northup, T. E., Birnbaum, K. M., Boca, A., Boozer, A. D., and Kimble, H. J. Trapped Atoms in Cavity QED: Coupling Quantized Light and Matter. *J. Phys. B: At. Mol. Opt. Phys.* **38**, S551-S565 (2005).

³ Thompson, R. J., Rempe, G., and Kimble, H. J. Observation of normal-mode splitting for an atom in an optical cavity. *Phys. Rev. Lett.* **68**, 1132 (1992).

⁴ Wallraff, A., Schuster, D. I., Blais, A., Frunzio, L., Huang, R.-S., Majer, J., Kumar, S., Girvin, S. M., and Schoelkopf, R. J. Strong coupling of a single photon to a superconduct-

- ing qubit using circuit quantum electrodynamics. *Nature (London)* **431**, 162 (2004).
- ⁵ Reithmaier, J. P., Sek, G., Löffler, A., Hofmann, C., Kuhn, S., Reitzenstein, S., Keldysh, L. V., Kulakovskii, V. D., Reinecke, T. L., and Forchel, A. Strong coupling in a single quantum dot-semiconductor microcavity system. *Nature (London)* **432**, 197 (2004).
 - ⁶ Yoshie, T., Scherer, A., Hendrickson, J., Khitrova, G., Gibbs, H. M., Rupper, G., Ell, C., Shchekin, O. B., and Deppe, D. G. Vacuum Rabi splitting with a single quantum dot in a photonic crystal nanocavity. *Nature (London)* **432**, 200 (2004).
 - ⁷ Blais, A., Huang, R.-S., Wallraff, A., Girvin, S. M., and Schoelkopf, R. J. Cavity quantum electrodynamics for superconducting electrical circuits: An architecture for quantum computation. *Phys. Rev. A* **69**, 062320 (2004).
 - ⁸ Devoret, M., Girvin, S., and Schoelkopf, R. J. Circuit-QED: How strong can the coupling between a Josephson junction atom and a transmission line resonator be? *Ann. Phys. (Leipzig)* **16**, 767 (2007).
 - ⁹ Schoelkopf, R. J. and Girvin, S. M. Wiring up quantum systems. *Nature (London)* **451**, 664 (2008).
 - ¹⁰ Schreier, J. A., Houck, A. A., Koch, J., Schuster, D. I., Johnson, B. R., Chow, J. M., Gambetta, J. M., Majer, J., Frunzio, L., Devoret, M. H., Girvin, S. M., and Schoelkopf, R. J. Suppressing charge noise decoherence in superconducting charge qubits. *Phys. Rev. B* **77**, 180502 (2008).
 - ¹¹ Zhu, Y., Gauthier, D. J., Morin, S. E., Wu, Q., Carmichael, H. J., and Mossberg, T. W. Vacuum Rabi splitting as a feature of linear-dispersion theory: Analysis and experimental observations. *Phys. Rev. Lett.* **64**, 2499 (1990).
 - ¹² Tian, L. and Carmichael, H. J. Quantum trajectory simulations of the two-state behavior of an optical cavity containing one atom. *Phys. Rev. A* **46**, R6801 (1992).
 - ¹³ Brune, M., Schmidt-Kaler, F., Maali, A., Dreyer, J., Hæggley, E., Raimond, J. M., and Haroche, S. Quantum Rabi Oscillation: A Direct Test of Field Quantization in a Cavity. *Phys. Rev. Lett.* **76**, 1800 (1996).
 - ¹⁴ Schuster, I., Kubanek, A., Fuhrmanek, A., Puppe, T., Pinkse, P. W. H., Murr, K., and Rempe, G. Nonlinear spectroscopy of photons bound to one atom. *Nature Physics* **4**, 382 (2008).
 - ¹⁵ Birnbaum, K. M., Boca, A., Miller, R., Boozer, A. D., Northup, T. E., and Kimble, H. J. Photon blockade in an optical cavity with one trapped atom. *Nature (London)* **436**, 87 (2005).
 - ¹⁶ Fink, J. M., Göppl, M., Baur, M., Bianchetti, R., Leek, P. J., Blais, A., and Wallraff, A. Climbing the Jaynes-Cummings ladder and observing its nonlinearity in a cavity QED system. *Nature (London)* **454**, 315 (2008).
 - ¹⁷ Hofheinz, M., Weig, E. M., Ansmann, M., Bialczak, R. C., Lucero, E., Neeley, M., O’Connell, A. D., Wang, H., Martinis, J. M., and Cleland, A. N. Generation of Fock states in a superconducting quantum circuit. *Nature (London)* **454**, 310 (2008).
 - ¹⁸ Simmonds, R. et al. (unpublished)
 - ¹⁹ Deppe, F., Mariani, M., Menzel, E., Marx, A., Saito, S., Kakuyanagi, K., Tanaka, H., Meno, T., Semba, K., Takayanagi, H., Solano, E., and Gross, R. Two-photon Probe of the Jaynes-Cummings Model and Symmetry Breaking in Circuit QED. *arXiv:0805.3294* (2008).
 - ²⁰ Koch, J., Yu, T. M., Gambetta, J., Houck, A. A., Schuster, D. I., Majer, J., Blais, A., Devoret, M. H., Girvin, S. M., and Schoelkopf, R. J. Charge-insensitive qubit design derived from the Cooper pair box. *Phys. Rev. A* **76**, 042319 (2007).
 - ²¹ Bouchiat, V., Vion, D., Joyez, P., Esteve, D., and Devoret, M. H. Quantum Coherence with a Single Cooper Pair. *Physica Scripta* **T76**, 165 (1998).
 - ²² Walls, D. and Milburn, G. *Quantum Optics*. Springer, 2nd edition (1995).
 - ²³ Carmichael, H. J. *Statistical Methods in Quantum Optics 2: Non-Classical Fields*. Springer (2008).
 - ²⁴ Houck, A. A., Schreier, J. A., Johnson, B. R., Chow, J. M., Koch, J., Gambetta, J. M., Schuster, D. I., Frunzio, L., Devoret, M. H., Girvin, S. M., and Schoelkopf, R. J. Controlling the spontaneous emission of a superconducting transmon qubit. *arXiv:0803.4490* (2008).

Acknowledgments

This work has been supported by Yale University via a Quantum Information and Mesoscopic Physics Fellowship (AAH, JK), the LPS/NSA-ARO grant W911NF-05-1-0365, NSF grants DMR-0653377, DMR-0603369, and PHY-0653073, and by Academy of Finland. We thank J. Gambetta, A. Blais, and A. Wallraff for helpful discussions, and L. Frunzio and B. Johnson for fabrication of the sample.

Author contributions

JMC led the experimental effort. LSB and JK performed the calculations and did most of the writing. AAH gave technical support and conceptual advice. ET contributed to the early theory. MHD, SMG, and RJS provided support and supervised the project.

Author information

Correspondence and requests for materials should be addressed to RJS.